Published by The College of Science & Information Technology (COSIT), TASUED, Vol. 19, No. 1, pp. 10-22.

**COSIT, TASUED**
**Journal of Science and Information Technology (JOSIT)**

# Benzotrithiophene Derivative as a Corrosion Inhibitor: Insights from Density Functional Theory and Monte Carlo Simulation Studies

**Badeji, A. A.**

*Department of Chemical Sciences, Tai Solarin University of Education, Ijagun, Ogun State, Nigeria*
*Corresponding Author: ogunlanaaa@tasued.edu.ng*

**Abstract**

This study presents a comprehensive theoretical investigation into the corrosion inhibition efficiency of benzo[1,2-b:3,4-b':5,6-b"]trithiophene (BTH) on iron surfaces using density functional theory (DFT) and Monte Carlo (MC) simulations. The molecular geometry, electronic structure, and reactivity descriptors of BTH were explored in both gas and solvent environments (DMSO, $H_2O$, ethanol) at the wB97XD/6-311++G(2d,2p) level of theory. Geometry optimization and vibrational frequency analyses indicated that BTH maintains a stable molecular structure regardless of the solvent. Natural Bond Orbital (NBO) analysis revealed significant donor–acceptor interactions, especially in polar solvents, suggesting enhanced electron delocalization and stabilization. Molecular electrostatic potential (MESP) maps and electrophilicity indices confirmed BTH's increased electron-accepting capacity in polar media. Quantum chemical descriptors such as HOMO-LUMO gap, ionization potential, and softness affirmed BTH's suitability as an efficient electron donor and moderate electrophile. Monte Carlo simulations of BTH adsorption on the Fe(110) surface showed strong and stable interactions in both gas (adsorption energy = –121.88 kcal/mol) and solution phases (adsorption energy = –2819.34 kcal/mol), with stronger binding and larger deformation in the solvated environment. These findings confirm that BTH exhibits significant promise as a corrosion inhibitor in both dry and acidic media.

**Keywords:** Benzotrithiophene derivative (BTH), Corrosion inhibitor, DFT calculations, Monte Carlo Simulation

## INTRODUCTION

Corrosion of metals, particularly in harsh industrial environments, poses a significant challenge that affects numerous industries, including oil and gas, marine engineering, and chemical processing. It leads to material degradation, substantial economic losses, safety hazards, and environmental concerns. To mitigate its effects, effective solutions are essential (Assad et al., 2025; Bender et al., 2022; Odeyemi & Alaba, 2025). One common and efficient approach is the use of corrosion inhibitors. Among the various classes of inhibitors, organic compounds containing heteroatoms (such as sulfur, nitrogen, and oxygen) have garnered significant attention due to their ability to adsorb onto metal surfaces and form protective barriers that reduce corrosion rates (Verma et al., 2021; Zhang et al., 2023). The growing demand for more efficient and environmentally friendly corrosion inhibitors necessitates the exploration of novel compounds with improved performance and lower toxicity (Ahmed et al., 2024). While many existing inhibitors are effective, their practical application is often limited by issues related to sustainability, environmental compatibility, and long-term efficiency (Kadhim et al., 2021; She et al., 2024).

Benzotrithiophene, a sulfur-rich heterocyclic compound, has recently attracted attention as a potential corrosion inhibitor, particularly in acidic media (Rossi et al., 2017). Its molecular structure, characterized by three sulfur atoms integrated within a conjugated system, enhances its ability to adsorb strongly onto metal surfaces, thereby inhibiting oxidation and metal degradation (Pan et al., 2021). Moreover, benzotrithiophene has been studied extensively for its roles in organic electronics, including organic photovoltaic cells, perovskite solar cells, and field-effect transistors, due to its notable stability, planar structure,

**Cite as:**

Badeji, A. A. (2025). Benzotrithiophene Derivative as a Corrosion Inhibitor: Insights from DFT and Monte Carlo Simulation Studies. *Journal of Science and Information Technology (JOSIT)*, Vol. 19, No. 1, pp. 10-22.

extended π-conjugation, and excellent hole-transporting properties. For instance, benzotrithiophene-based conjugated microporous polymers have demonstrated tunable band gaps and efficient visible-light-induced photocatalytic activity, highlighting their potential as metal-free photocatalysts and electronic materials (Han et al., 2021). Small-molecule benzotrithiophene derivatives have also been successfully used as hole-transporting materials (HTMs) in perovskite solar cells, achieving high power conversion efficiencies and good long-term stability (Budiawan et al., 2020; Garcia-Benito et al., 2021). Furthermore, recent reviews summarize advances in benzotrithiophene-based semiconductors, underlining their versatility and promise in organic solar cells and organic field-effect transistors (Patra & Park, 2022). This dual functionality, as both a high-performance organic electronic material and a corrosion inhibitor, positions benzotrithiophene as a promising multifunctional compound for industrial use. Despite its potential, the specific mechanisms by which benzotrithiophene interacts with metal surfaces remain inadequately understood. Enhancing its inhibitory efficiency calls for a deeper investigation of its adsorption behavior, molecular interactions, and electronic properties.

Computational methods such as density functional theory (DFT) and Monte Carlo (MC) simulations provide powerful frameworks for studying molecular-level interactions between corrosion inhibitors and metal surfaces (Murmu et al., 2022). These techniques enable the prediction of adsorption energies, charge distribution, and reactivity descriptors, offering key insights into the structure–activity relationships that govern inhibition efficiency.

Additionally, quantum chemical analysis and MC-based adsorption modeling help identify the most favorable adsorption configurations, which are crucial for guiding the development of improved inhibitors (Kasprzhitskii & Lazorenko, 2021). In this study, DFT calculations and Monte Carlo simulations are employed to explore the inhibitory behavior of benzo[1,2-b:3,4-b':5,6-b"]trithiophene (BTH), a benzotrithiophene derivative (Figure 1). BTH was selected for this study due to its unique electronic structure, which combines a conjugated π-system with multiple sulfur atoms capable of strong donor–acceptor interactions with metal surfaces. Sulfur-containing heterocycles are well-documented for their high adsorption affinity toward transition metals, enabling the formation of stable protective films. The rigid planar geometry of BTH also facilitates π–π stacking and surface alignment, enhancing its corrosion inhibition potential. Unlike conventional inhibitors that may degrade in aggressive environments, the extended aromatic framework of BTH offers superior chemical stability and environmental resilience.

This work specifically targets corrosion inhibition in acidic environments, such as hydrochloric acid media used in industrial pickling, descaling, and oil well acidizing operations, where steel is highly susceptible to electrochemical attack. These conditions are common in sectors such as petroleum, chemical processing, and marine engineering, where effective corrosion protection is essential for reducing maintenance costs, minimizing downtime, and extending equipment lifespan. By investigating BTH's adsorption and electronic properties under both gas-phase and solvent-phase conditions, this study aims to provide insights into its adsorption characteristics, interaction mechanisms, and electronic properties that contribute to corrosion inhibition. The findings from this work not only enhance our understanding of BTH's inhibitory mechanism but also provide a basis for future experimental validation and the design of more effective, environmentally sustainable corrosion inhibitors for industrial applications.

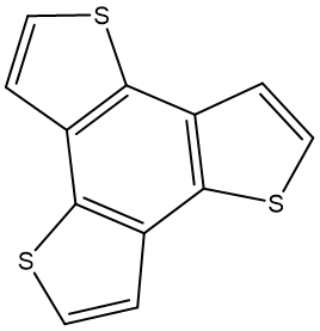


**Figure 1.** 2D diagram of benzo[1,2-b:3,4-b':5,6-b"]trithiophene (BTH).

## COMPUTATIONAL METHOD

This study employed both density functional theory (DFT) and Monte Carlo (MC) simulations to investigate the corrosion inhibition potential of BTH. All DFT computations were performed with the Gaussian 16W suites (Frisch et al., 2016) on the Lengau cluster at the Centre for High Performance Computing (CHPC), South Africa. Monte Carlo simulations were conducted using the Adsorption Locator module in Materials Studio 6.0.

**DFT Studies**

The structural and electronic properties of BTH were examined using density functional theory (DFT). The initial molecular structure was generated and visualized using GaussView 6.0.16 (Dennington et al., 2023), which also facilitated the construction of input files for the calculations. Geometry optimization was carried out in the gas phase using the wB97XD functional (Chai & Head-Gordon, 2008) in conjunction with the 6-311++G(2d,2p) basis set for all atoms. The wB97XD functional is a long-range corrected hybrid functional that includes empirical dispersion corrections. This makes it especially suitable for accurately modeling non-covalent interactions, such as π–π stacking and adsorption processes, which are critical features in corrosion inhibition mechanisms. Its ability to account for long-range electron correlation and dispersion forces ensures reliable predictions of molecular geometry and interaction energies in complex systems like inhibitor-metal interfaces (Bhatta et al., 2015; Mardirossian & Head-Gordon, 2017).

The 6-311++G(2d,2p) basis set is a triple-zeta split-valence basis set augmented with diffuse functions and polarization functions on all atoms. The diffuse functions improve the description of electron distribution in anionic species or molecules with lone pairs, while the polarization functions enhance flexibility in modeling electron cloud distortions, particularly important for accurately simulating reaction intermediates, dipole moments, and frontier molecular orbitals involved in adsorption (Wiberg, 2004).

Vibrational frequency analysis was conducted to verify that the optimized geometry corresponds to a true energy minimum, as indicated by the absence of imaginary frequencies (El-Azhary & Suter, 1996). To account for solvent effects, single-point energy (SPE) calculations were subsequently performed on the gas-phase optimized structure using the SMD solvation model (Marenich et al., 2009) and dimethylsulfoxide (DMSO), ethanol, and water as solvents. All 3D structural representations of BTH were rendered using Chemcraft software (Andrienko, 2010).

**Quantum Chemical Descriptors**

Using the DFT-optimized geometries, several quantum chemical descriptors were extracted to assess the reactivity and inhibition efficiency of BTH. These descriptors are described below. The Highest Occupied Molecular Orbital (HOMO) energy indicates the molecule's ability to donate electrons, whereas the Lowest Unoccupied Molecular Orbital (LUMO) energy reflects its capacity to accept electrons. A higher energy of the HOMO ($E_{HOMO}$) suggests better electron-donating ability, which is favorable for forming coordinate bonds with vacant d-orbitals of metal atoms (Aihara, 1999). Conversely, a lower energy of the LUMO ($E_{LUMO}$) indicates a greater tendency to accept electrons from the metal surface, enhancing the likelihood of back-donation interactions. Thus, the position of these orbitals plays a central role in adsorption and bonding interactions at the metal-inhibitor interface. Next, the energy gap ($\Delta E$) represents the molecular chemical stability and reactivity, and it is computed using eq. (1) below. A smaller ΔE implies higher chemical reactivity and lower kinetic stability, facilitating the interaction between the inhibitor and the metal surface (Minsky et al., 1985). In corrosion inhibition, molecules with lower energy gaps are often more reactive, enhancing their ability to adsorb effectively on metallic surfaces and form protective films.

$$\text{Energy gap } (\Delta E = E_{\text{LUMO}} - E_{\text{HOMO}}) \qquad (1)$$

Based on Koopmans' theorem, the ionization potential (IP) is approximated as the negative of ($-E_{HOMO}$), and the electron affinity (EA) is approximated as the negative of ($-E_{LUMO}$). IP indicates the energy required to remove an electron from the molecule, and EA reflects the energy released when the molecule gains an electron. Molecules with lower IP are more willing to donate electrons, enhancing their nucleophilicity, while higher EA values imply a greater ability to accept electrons, relevant for electrophilic interactions (Su et al., 2011). Global hardness quantifies the resistance of the molecule to change its electron distribution. A hard molecule resists deformation of its electron cloud, while a soft molecule can easily polarize and participate in charge transfer (Zhan et al., 2003). Softness, the reciprocal of hardness ($\sigma = 1/2\eta$), describes the polarizability and chemical reactivity of a molecule. A soft molecule (lower η, higher σ) is generally more chemically reactive and interacts more readily with a metal surface (Franco-Pérez et al., 2018; S. Oladipo et al., 2024). The value for the hardness and softness for BTH was computed using eq. (2) given below Global hardness (η) and softness (σ):

$$\left(\eta = \frac{IP - E.A}{2}, \sigma = \frac{1}{2\eta}\right) \qquad (2)$$

Electronegativity reflects the tendency of a molecule to attract electrons towards itself. A high χ value suggests strong electron-withdrawing capability (Iczkowski & Margrave, 1961). The electrophilicity index ($\omega = \chi^2/2\eta$) provides a measure of the stabilization in energy when the system acquires additional electronic charge from the environment. Higher ω values indicate stronger electrophilic character, making the molecule more effective at accepting electrons from the metal surface, facilitating inhibitor–metal interaction through back-donation (Pal & Chattaraj, 2023). The values for the electronegativity and electrophilicity index were computed using eq. (3) below. Electronegativity (χ) and electrophilicity index:

$$(\omega)\ (\chi = \frac{IP+E.A}{2},\ \omega = \frac{u^2}{2\eta}) \qquad (3)$$

These descriptors were calculated based on Koopmans' theorem (Tsuneda et al., 2010) and used to interpret the electronic behavior of the inhibitor, including its interaction tendencies with metal surfaces.

**Monte Carlo (MC) Simulation**

Monte Carlo simulations were carried out using the Adsorption Locator module within Materials Studio 6.0 (Accelrys Inc., USA). The aim is to determine the adsorption energy of BTH on the Fe (110) surface. The COMPASS force field was applied to describe molecular interactions (Sun et al., 1998). A clean Fe (110) surface was cleaved from the Fe crystal structure and subsequently optimized to reach an energy minimum. This surface was then extended to an 8 × 8 supercell, and a vacuum slab of 6.0 nm thickness was added above the surface to mimic realistic boundary conditions. The Metropolis Monte Carlo method was employed to perform simulated annealing, enabling exhaustive sampling of possible adsorption configurations of BTH on the iron surface. The resulting adsorption energy and the most stable configurations provided insight into the strength and nature of inhibitor-metal interactions.

## RESULTS AND DISCUSSION

### DFT studies

#### 1. Geometry optimization:

The geometry optimization of BTH was carried out by DFT calculations. The 3D structure, as represented in Figure 2, showed the key structural components (C-S, C-H, and C=C bonds) of the compound. In this geometry, the benzene ring is fused to three thiophene groups.

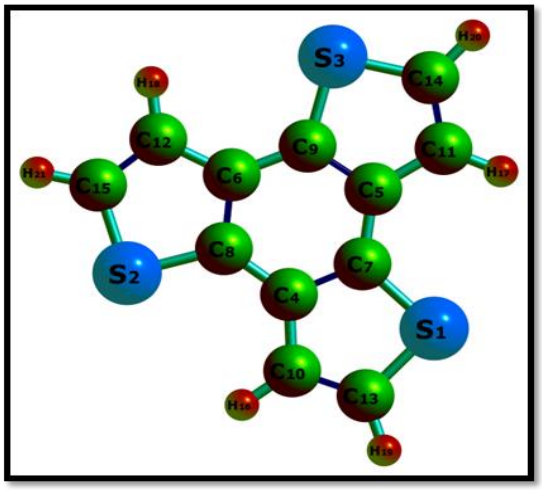


Figure 2. Geometry optimization plot of BTH

Meanwhile, the bond lengths of BTH in various solvents (DMSO, ethanol, $H_2O$) and the gas phase is given in Table 1 below. The C-S bond length remains consistent at 1.73 Å across all environments. This implies that the solvent environment has no impact on the C–S bond i.e., the electronic density or bonding nature of the C–S bond in BTH is relatively independent of solvent polarity. The C–H bond length is also invariant at 1.08 Å in all the studied environments. This constancy indicates that hydrogen bonding interactions or electrostatic effects involving C-H are negligible. This is because C–H bonds do not participate in strong hydrogen bonding unless the carbon is adjacent to highly electronegative atoms (e.g., in –CHO, -$CH_2F$ groups). Since the C–H in BTH is not significantly polarized, its interaction with solvent molecules is minimal, resulting in unchanged bond lengths. The C=C bond length exhibits slight variability: in DMSO and $H_2O$, it is 1.43 Å, whereas in ethanol and the gas phase, it is marginally shorter at 1.42 Å. Although the difference is small, it may arise from subtle changes in the electronic distribution within the conjugated π-system of BTH. In more polar solvents (Hernandezperni & Leuenberger, 2005)

such as DMSO and $H_2O$, solvent–molecule interactions can induce polarization of the π-electron cloud, causing partial delocalization over adjacent atoms.

**Table 1.** Optimized bond lengths (Å) of BTH in various solvent environments, and gas phase

| Compounds | C-S (Å) | C-H (Å) | C=C (Å) |
|---|---|---|---|
| BTH-DMSO | 1.73 | 1.08 | 1.43 |
| BTH-Ethanol | 1.73 | 1.08 | 1.42 |
| BTH-$H_2O$ | 1.73 | 1.08 | 1.43 |
| BTH-Gas | 1.73 | 1.08 | 1.42 |

This slightly reduces the pure double-bond character of the C=C linkage, leading to a marginally longer bond length. In contrast, in less polar environments such as ethanol and the gas phase, there is reduced solvent-induced polarization, allowing the π-electrons to remain more localized between the two carbon atoms. This enhances the double-bond character, slightly strengthening the bond and shortening the bond length. The uniformity of the C–S and C–H bonds, combined with the minimal variations in the C=C bond, indicates that BTH possesses a stable geometry largely independent of solvent interactions.

## 2. Vibrational studies:

The vibrational analysis of BTH across different solvents (DMSO, ethanol, $H_2O$) and in the gas phase highlights subtle solvent effects on its molecular vibrations (Table 2). For symmetric CH=CH stretching, frequencies slightly increase as the solvent polarity decreases, with the highest values observed in the gas phase (3270.47–3269.90 $cm^{-1}$) and the lowest in DMSO (3265.81–3259.89 $cm^{-1}$). This trend suggests stronger stabilization of the symmetric stretching vibration in polar solvents. Similarly, for asymmetric CH=CH stretching, the frequencies are moderately higher in $H_2O$ (3232.23–3228.76 $cm^{-1}$) compared to DMSO (3229.49–3226.33 $cm^{-1}$), reflecting solvent interactions dampening the vibrational energy (Crandall, 1970). The scissoring C=C mode shows minimal variation across all environments, with slightly higher frequencies in the gas phase (1624.19–1550.90 $cm^{-1}$) compared to the solvents (~1621.52–1550.11 $cm^{-1}$), indicating limited solvent interaction with this mode. The rocking CH=CH mode also shows slight frequency increases in less polar environments, with the gas phase exhibiting the highest values (1446.61–1406.51 $cm^{-1}$) and solvents (1442.75–1402.67 $cm^{-1}$) demonstrating stabilization. Conversely, for the wagging CH=CH mode, the gas phase frequencies (919.88–917.61 $cm^{-1}$) are lower than those in solvents (933.95–924.42 $cm^{-1}$), suggesting enhanced stabilization by solvent interactions. Finally, the symmetric C-S stretching mode exhibits higher frequencies in the gas phase (674.19–664.58 $cm^{-1}$) compared to solvents (670.97–670.02 $cm^{-1}$), indicating weaker stabilization of this mode in polar environments.

In general, the results show that solvent polarity has a subtle yet distinct impact on the vibrational behavior of BTH, stabilizing most vibrational modes and slightly lowering their frequencies compared to the gas phase.

**Table 2.** Frequencies of BTH and vibrational modes in different solvents

| Assignments | BTH-DMSO ($cm^{-1}$) | BTH-Ethanol ($cm^{-1}$) | BTH-$H_2O$ ($cm^{-1}$) | BTH-Gas ($cm^{-1}$) |
|---|---|---|---|---|
| Symmetric CH=CH | 3265.81,3265.23, 3259.89 | 3267.85,3265.08, 3261.40 | 3269.67,3268.60, 3263.56 | 3270.47,3270.07, 3269.90 |
| Asymmetric CH=CH | 3229.49,3226.88, 3226.33 | 3228.42,3226.85, 3224.79 | 3232.23,3229.39, 3228.76 | 3229.76,3229.50, 3229.39 |
| Scissoring C=C | 1620.97,1620.39, 1550.71 | 1621.52,1621.23, 1550.40 | 1621.09,1620.45, 1550.11 | 1624.19,1623.71, 1550.90 |
| Rocking CH=CH | 1442.75,1405.28, 1402.62 | 1443.37,1406.62, 1403.43 | 1442.87,1405.69, 1402.67 | 1446.61,1410.77, 1406.51 |
| Wagging CH=CH | 933.77, 930.28, 926.53 | 933.45, 931.19, 924.42 | 933.95, 930.63, 926.91 | 919.88, 919.43, 917.61 |

## 3. NBO studies:

According to Table 3, the NBO analysis of BTH across different environments (DMSO, ethanol, $H_2O$, and gas phase) provides insights into electronic interactions, perturbation energies ($E^2$), energy differences ($E(j)-E(i)$), and coupling constants ($F(i,j)$). In DMSO, significant interactions include the $\sigma(C_{12}-C_{15})\rightarrow\sigma*(C_{10}-H_{16})$ with $E^2$=1065.18kJ/mol, $E(j)-E(i)$=0.30, and $F(i,j)$=0.507, alongside $\sigma(S_2-C_{15})\rightarrow\sigma(C_{10}-H_{16})$, which shows a higher $E^2$=1129.04 kJ/mol, suggesting strong stabilization due to electron

donation from the sulfur-carbon bond (Inah et al., 2025). In ethanol, notable interactions include $\pi(C_6–C_8)\rightarrow\sigma(C_5–C_7)$ with the highest $E^2$=1166.54 kJ/mol $E(j)–E(i)$=0.46, and $F(i,j)$=0.700, indicating significant delocalization involving the C=C π-electrons. The $(S_2–C_{15})\rightarrow\sigma(C_{10}–H_{16})$ $E^2$=1183.58 kJ/mol with a smaller $E(j)–E(i)$=0.12, showing strong sulfur-carbon bond contributions.

**Table 3.** Perturbation energies ($E^2$kj/mol), interactions types, energy differences (E(j)-E(i)) and coupling constant (F(i,j)) of BTH.

| Compounds | Donor (i) | Acceptor (j) | $E^2$ (kj/mol) | E(j)-E(i) | F(i,j) |
|---|---|---|---|---|---|
| **BTH-DMSO** | $\sigma C_{12}$ - $C_{15}$ | $\sigma^* C_{10}$ - $H_{16}$ | 1065.18 | 0.30 | 0.507 |
| | $\sigma S_2$ - $C_{15}$ | $\sigma$ $C_{10}$ - $H_{16}$ | 1129.04 | 0.13 | 0.337 |
| **BTH-Ethanol** | $\pi C_6$ - $C_8$ | $\sigma C_5$ - $C_7$ | 1166.54 | 0.46 | 0.700 |
| | $\sigma S_2$ - $C_{15}$ | $\sigma C_{10}$ - $H_{16}$ | 1183.58 | 0.12 | 0.338 |
| **BTH-$H_2O$** | $\pi C_6$ - $C_8$ | $\sigma^* C_5$ - $C_7$ | 1143.58 | 0.47 | 0.698 |
| | $\sigma S_2$ - $C_{15}$ | $\sigma^* C_{10}$ - $H_{16}$ | 1105.13 | 0.13 | 0.336 |
| **BTH-Gas** | $\pi C_{11}$ - $C_{14}$ | $\sigma^* C_{12}$ - $C_{15}$ | 770.02 | 172.10 | 27.270 |
| | $\sigma C_{11}$ - $C_{14}$ | $\sigma C_6$ - $C_8$ | 799.70 | 1.75 | 1.061 |

In $H_2O$, the $\pi(C_6–C_8) \rightarrow \sigma*(C_5–C_7)$ interaction is slightly weaker than in ethanol $E^2$ = 1143.58kJ/mol, $E(j) - E(i)$ = 0.47, and $F(i,j)$ = 0.698, while $\sigma(S_2–C_{15}) \rightarrow \sigma*(C_{10}–H_{16})$ retains stability ($E^2$ = 1105.13kJ/mol) with minimal energy difference $E(j) - E(i)$ = 0.13. In the gas phase, the interactions differ significantly. The $(C_{11}–C_{14}) \rightarrow \sigma*(C_{12}–C_{15})$ shows $E^2$ = 770.02kJ/mol but with a massive $E(j) - E(i)$ = 172.10, reflecting weak coupling ($F(i,j)$ = 27.270. Similarly, $(C_{11}–C_{14}) \rightarrow \sigma(C_6–C_8)$ has $E^2$ = 799.70 kJ/mol, $E(j)–E(i)$=1.75, implying reduced stabilization compared to solvent environments. In general, solvents enhance electron delocalization and stabilize specific donor-acceptor interactions compared to the gas phase, with ethanol and $H_2O$ showing stronger π-type interactions, while DMSO stabilizes σ-type interactions involving sulfur bonds.

## 4. Molecular Electrostatic Potential:

The Molecular Electrostatic Potential (MESP) plots of BTH in various environments (gas, DMSO, ethanol, and $H_2O$) illustrate the distribution of electronic charge across the molecule, which helps to identify regions of electrophilic and nucleophilic character. The electrophilicity index (ω) values provide insight into the compound's ability to accept electrons (Parr et al., 1999). The red regions correspond to electron-rich areas (nucleophilic), such as those near electronegative atoms or π-electron systems. The blue regions correspond to electron-deficient areas (electrophilic), likely around hydrogen atoms or other electron-poor regions (Tsuneda et al., 2010). The electrophilicity index (ω) increases slightly in polar solvents compared to the gas phase. In the gas phase, ω=1.489eV, while it increases to ω=1.498eV in ethanol, ω=1.502eV in DMSO, and ω=1.503eV in $H_2O$. This trend suggests that BTH has enhanced electrophilic behavior in polar solvents due to solvent stabilization of its electronic density (Figure 3).

Color differences in the MESP plots show that the gas phase plot shows relatively lighter shades of red and blue, indicating a balanced distribution of electron density without significant polarization. In DMSO, the deeper red regions become more prominent, particularly around the sulfur atoms, reflecting an increased electron density in these areas due to the polar nature of DMSO. The red and blue regions are slightly more pronounced compared to the gas phase, indicating moderate polarization effects from the ethanol solvent. The MESP plot in water shows the most prominent red regions, reflecting significant solvent stabilization of electron-rich regions due to water's strong polar nature.

The increase in the electrophilicity index from gas to polar solvents suggests that BTH becomes more reactive towards nucleophiles in polar environments. The deeper red areas in the polar solvents indicate enhanced stabilization of nucleophilic sites, which is vital for understanding the compound's behaviour in reactions such as hydrogen bonding, charge transfer, or nucleophilic attacks (Anzovino & Bretz, 2016). Conversely, the consistent presence of blue regions across all environments suggests a stable electrophilic character, particularly at electron-deficient sites. Therefore, the MESP plots and the corresponding ω values highlight how solvent

polarity modulates the reactivity and electronic distribution of BTH, with polar solvents enhancing its electrophilic nature and stabilizing nucleophilic sites.

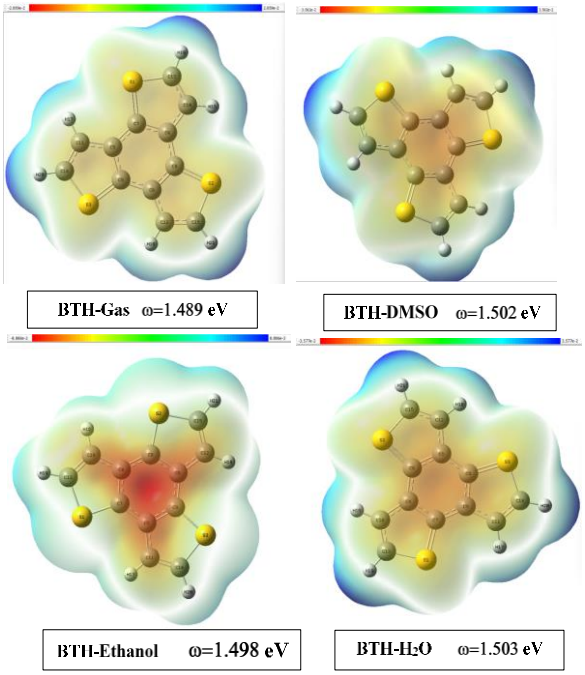


**Figure 3.** MESP plots of BTH in different solvents.

## 5. Quantum chemical descriptors:

The quantum chemical descriptors of the BTH were analyzed in various environments—DMSO, ethanol, water, and gas phase—using Density Functional Theory (DFT). Key descriptors evaluated include the energies of the frontier molecular orbitals ($E_{HOMO}$ and $E_{LUMO}$), energy gap (ΔE), ionization potential (IP), electron affinity (EA), chemical hardness (η), softness (σ), chemical potential (μ), electronegativity (χ), and electrophilicity index (ω) (Tsuneda et al., 2010). The values are shown in Table 4 below. The $E_{HOMO}$ values ranged from -7.781 to -7.803 eV, suggesting a strong tendency of the molecule to donate electrons to a metal surface. The $E_{LUMO}$ values, which fell between -0.666 and -0.682 eV, indicate a moderate ability to accept electrons. These stable orbital energy levels across solvents imply that the compound maintains consistent reactivity in different media.

Furthermore, the energy gap (ΔE), which reflects the kinetic stability and chemical reactivity of the molecule, was lowest in the gas phase (7.099 eV) and slightly higher in water (7.137 eV) (Figure 4). This small variation suggests that BTH possesses relatively high reactivity, particularly in nonpolar environments (Badeji et al., 2024; Matinise et al., 2025). The ionization potential (7.781–7.803 eV) and electron affinity (0.666–0.682 eV) remained consistent across all environments, reinforcing the molecule's stable electronic properties. The chemical hardness (η) values, ranging from 3.550 to 3.569 eV, indicate moderate resistance to charge transfer, while the softness (σ), around 0.140 $eV^{-1}$ (Table 4), confirms that the molecule is moderately soft—an advantageous feature for effective adsorption on metal surfaces ( Oladipo, S. D. et al., 2025). The chemical potential (μ) was negative in all environments, around -4.235 eV, reflecting the molecule's tendency to donate electrons spontaneously (Table 4). Electronegativity (χ) remained constant at approximately 4.235 eV, while the electrophilicity index (ω) ranged slightly, with the highest value observed in the gas phase (2.523 eV), suggesting a better electron-accepting capability in nonpolar conditions (Dulla, 2024; Kaya & Kaya, 2015; Pal & Chattaraj, 2023).

**Table 4.** Quantum chemical descriptors of BTH in different solvents.

| Compounds | $E_{LUMO}$ (eV) | $E_{HOMO}$ (eV) | ΔE (eV) | EA (eV) | IP (eV) | η (eV) | σ ($eV^{-1}$) | μ (eV) | χ (eV) | ω (eV) |
|---|---|---|---|---|---|---|---|---|---|---|
| BTH-DMSO | -0.668 | -7.801 | 7.133 | 0.668 | 7.801 | 3.567 | 0.140 | -4.235 | 4.235 | 2.514 |
| BTH-Ethanol | -0.673 | -7.797 | 7.124 | 0.673 | 7.797 | 3.562 | 0.140 | -4.235 | 4.235 | 2.518 |
| BTH-Water | -0.666 | -7.803 | 7.137 | 0.666 | 7.803 | 3.569 | 0.140 | -4.235 | 4.235 | 2.513 |
| BTH-Gas | -0.682 | -7.781 | 7.099 | 0.682 | 7.781 | 3.550 | 0.141 | -4.232 | 4.232 | 2.523 |

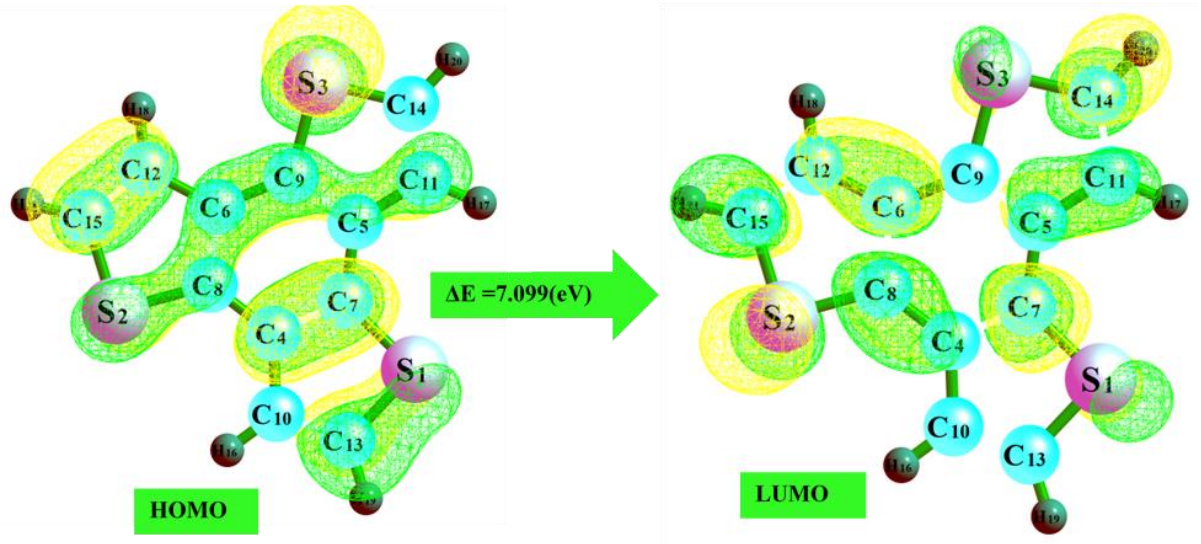


**Figure 4.** HOMO-LUMO plot of BTH in the gaseous state.

**Monte Carlo Simulation**

Monte Carlo (MC) simulations were employed to investigate the adsorption behavior and interaction strength of the BTH inhibitor molecule on the Fe (110) surface. This approach provides a statistical evaluation of the most stable adsorption configurations and associated energies, both in vacuum (gas phase) and in a simulated corrosive medium (solution phase) (Ramalingam & Santhi, 2024). By analyzing adsorption energies, deformation, and rigid adsorption contributions, the simulations offer critical insights into the thermodynamic feasibility and inhibition efficiency of BTH under different environmental conditions.

**Adsorption properties of inhibitor molecules**

The adsorption behavior of the BTH molecule on the Fe(110) surface was investigated using Monte Carlo simulations in both the gas and solvent phases. These simulations provide critical information on the interaction strength and stability of the inhibitor on the iron surface, which is vital in understanding its corrosion inhibition performance. In the gas phase, the simulation (Figure 5) shows that the BTH molecule is adsorbed parallel to the Fe (110) surface, maximizing surface coverage and interaction.

According to Table 5, the total energy obtained in this phase was 40.4189 kcal/mol, while the adsorption energy was calculated to be –121.8802 kcal/mol. The rigid adsorption energy, which assumes no structural relaxation, was slightly more negative at –122.5165 kcal/mol, indicating a strong and favorable adsorption process (Bourzi et al., 2020). The deformation energy, i.e., the energy required for the molecule to adjust its geometry during adsorption (Oukhrib et al., 2021), was found to be 0.6363 kcal/mol, signifying minimal structural distortion of the BTH molecule on adsorption (Table 5).

In the solution phase (Figure 6), a more realistic corrosion environment was simulated by introducing $H_2O$ and $Cl^-$ ions, representing an acidic medium such as HCl. Here, the BTH molecule retained a similar parallel adsorption configuration but with some solvation-induced adjustments. The total energy dropped significantly to –2819.341 kcal/mol, which reflects the influence of solvation effects (Xu et al., 2022). Notably, the adsorption energy in the solution phase remained very high (–2819.341 kcal/mol), while the rigid adsorption energy was even lower at –2880.166 kcal/mol. This sharp decrease illustrates enhanced stabilization of the inhibitor within the solvated environment. The corresponding deformation energy was 60.8249 kcal/mol, indicating more significant structural adaptation of the molecule when solvated compared to the gas phase (Omer et al., 2025).

The comparative visualization between the two systems (Figures 5 and 6) emphasizes the stronger and more dynamic interactions in the solvent phase. In particular, the presence of water molecules and chloride ions promotes competitive adsorption and subtle rearrangements of BTH on the Fe surface, enhancing its binding characteristics, thereby potentially improving its anticorrosive performance.

The results confirm that the BTH molecule has a high affinity for the Fe (110) surface under both dry and corrosive conditions, supporting its role as an effective corrosion inhibitor.

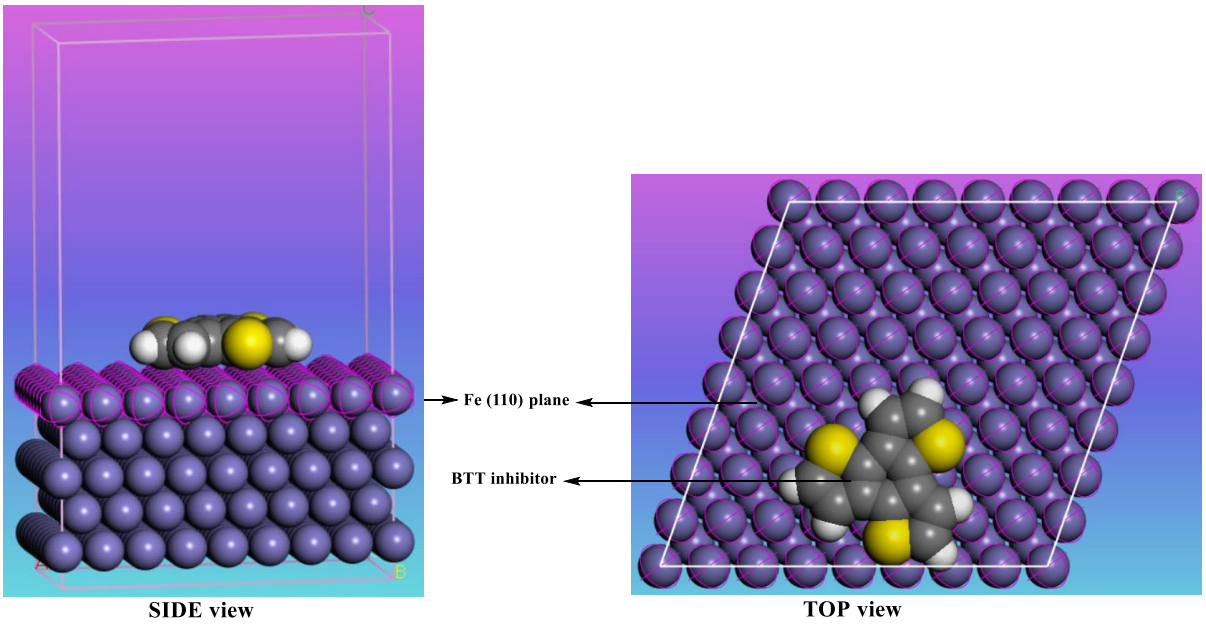


**Figure 5.** Optimized adsorption configuration of BTH inhibitor on Fe (110) surface in the gas phase. Side and top views showing the parallel orientation of the BTH molecule on the iron surface, indicating strong surface interaction in a vacuum environment.

**Table 5.** Adsorption parameters of BTH inhibitor on Fe (110) surface in gas and solution phases obtained from Monte Carlo simulations.

| | Total energy | Adsorption energy | Rigid adsorption energy | Deformation energy |
|---|---|---|---|---|
| Gas-phase | 40.41885424 | -121.88018227 | -122.51650983 | 0.63632757 |
| Solution-phase | -2.819341e+003 | -2.819341e+003 | -2.880166e+003 | 60.82489018 |

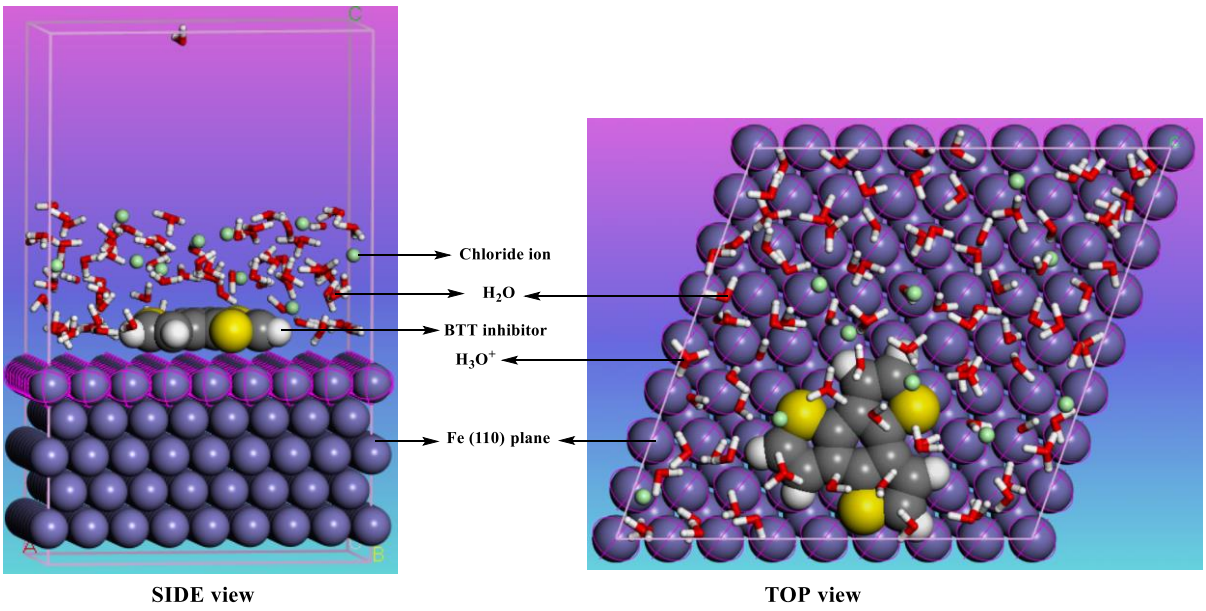


**Figure 6.** Optimized adsorption configuration of BTH inhibitor on Fe (110) surface in the presence of HCl (solution phase). Side and top views illustrating the interaction of BTH with the Fe surface under solvated conditions, including water molecules and chloride ions, simulating a corrosive environment.

## CONCLUSION

The combined DFT and Monte Carlo simulation results demonstrate that BTH is a highly stable and electronically favorable molecule for corrosion inhibition applications. Geometry optimization and vibrational analysis revealed that the molecular structure of BTH is largely unaffected by solvent polarity, highlighting its structural robustness. NBO results showed that polar solvents enhance key donor–acceptor interactions, particularly involving sulfur and π-bonds, while MESP mapping indicated increased nucleophilic and electrophilic character in polar environments. Frontier molecular orbital analysis confirmed strong electron-donating behavior (high $E_{HOMO}$), while the moderate energy gap and chemical softness support its reactivity and surface affinity. The increase in electrophilicity index in solvent environments further indicates BTH's readiness to accept electrons during metal-inhibitor interactions. Finally, Monte Carlo simulations confirmed that BTH adsorbs strongly on Fe(110) surfaces in both gas and corrosive (acidic) media, with stronger interaction and structural deformation observed in the latter. To sum up, BTH exhibits excellent adsorption characteristics, electronic reactivity, and environmental stability, establishing it as a promising candidate for corrosion protection in metal-based systems. Future work should involve experimental electrochemical and surface characterization studies to validate these computational predictions and explore the scalability of BTH-based inhibitors for industrial corrosion prevention in sectors such as marine, oil and gas, and infrastructure maintenance.

## REFERENCES


Ahmed, M. A., Amin, S., & Mohamed, A. A. (2024). Current and emerging trends of inorganic, organic and eco-friendly corrosion inhibitors. *RSC Advances*, *14*(43), 31877–31920.

Aihara, J. (1999). Reduced HOMO− LUMO gap as an index of kinetic stability for polycyclic aromatic hydrocarbons. *The Journal of Physical Chemistry A*, *103*(37), 7487–7495.

Andrienko, G. (2010). Chemcraft-graphical software for visualization of quantum chemistry computations. *See Https://Www. Chemcraftprog. Com*.

Anzovino, M. E., & Bretz, S. L. (2016). Organic chemistry students' fragmented ideas about the structure and function of nucleophiles and electrophiles: A concept map analysis. *Chemistry Education Research and Practice*, *17*(4), 1019–1029. https://doi.org/10.1039/C6RP00111D

Assad, H., Lone, I. A., Sharma, P. K., & Kumar, A. (2025). Corrosion in the Oil and Gas Industry. *Industrial Corrosion: Fundamentals, Failure, Analysis and Prevention*, 39–63.

Badeji, A. A., Omoniyi, M. T., Ogunbayo, T. B., Oladipo, S. D., & Akinbulu, I. A. (2024). Quantum chemical investigation of the degradation of acid orange 7 by different oxidants. *Discover Chemistry*, *1*(1), 55. https://doi.org/10.1007/s44371-024-00059-x

Bender, R., Féron, D., Mills, D., Ritter, S., Bäßler, R., Bettge, D., De Graeve, I., Dugstad, A., Grassini, S., & Hack, T. (2022). Corrosion challenges towards a sustainable society. *Materials and Corrosion*, *73*(11), 1730–1751.

Bhatta, R. S., Pellicane, G., & Tsige, M. (2015). Tuning range-separated DFT functionals for accurate orbital energy modeling of conjugated molecules. *Computational and Theoretical Chemistry*, *1070*, 14–20.

Bourzi, H., Oukhrib, R., El Ibrahimi, B., Abou Oualid, H., Abdellaoui, Y., Balkard, B., El Issami, S., Hilali, M., Bazzi, L., & Len, C. (2020). Furfural Analogs as Sustainable Corrosion Inhibitors—Predictive Efficiency Using DFT and Monte Carlo Simulations on the Cu(111), Fe(110), Al(111) and Sn(111) Surfaces in Acid Media. *Sustainability*, *12*(8), 3304. https://doi.org/10.3390/su12083304

Budiawan, W., Lai, K.-W., Karuppuswamy, P., Jadhav, T. S., Lu, Y.-A., Ho, K.-C., Wang, P.-C., Chang, C.-C., & Chu, C.-W. (2020). Asymmetric benzotrithiophene-based hole transporting materials provide high-efficiency perovskite solar cells. *ACS Applied Materials & Interfaces*.

Chai, J.-D., & Head-Gordon, M. (2008). Long-range corrected hybrid density functionals with damped atom–atom dispersion corrections. *Physical Chemistry Chemical Physics*, *10*(44), 6615. https://doi.org/10.1039/b810189b

Crandall, S. H. (1970). The role of damping in vibration theory. *Journal of Sound and Vibration*, *11*(1), 3-IN1. https://doi.org/10.1016/S0022-460X(70)80105-5

Dennington, R., Keith, T., & Millam, J. (2023). GaussView, Version 6.0. 1.6, Semichem Inc., Shawnee Mission, KS, 2016. *There Is No Corresponding Record for This Reference*.

Dulla, H. (2024). The Effect of Global and Local Chemical Reactivity Descriptors in the Determination of Properties of Transition Metal Clusters. *SINET: Ethiopian Journal of Science*, *46*(3), 296–305. https://doi.org/10.4314/sinet.v46i3.6

El-Azhary, A., & Suter, H. (1996). Comparison between optimized geometries and vibrational frequencies calculated by the DFT methods. *The Journal of Physical Chemistry*, *100*(37), 15056–15063.

Franco-Pérez, M., Polanco-Ramírez, C. A., Gázquez, J. L., & Ayers, P. W. (2018). Local and nonlocal counterparts of global descriptors: The cases of chemical softness and hardness. *Journal of Molecular Modeling*, *24*(10), 285. https://doi.org/10.1007/s00894-018-3823-4

Frisch, M., Trucks, G., Schlegel, H., Scuseria, G., Robb, M., Cheeseman, J., Scalmani, G., Barone, V., Petersson, G., & Nakatsuji, H. (2016). Gaussian 16 Revision C. 01, 2016. *Gaussian Inc. Wallingford CT*, *1*, 572.

Garcia-Benito, I., Urieta-Mora, J., Molina-Ontoria, A., & Martín, N. (2021). Chalcogen-containing hole transporting materials. *Bulletin of the Chemical Society of Japan*, *94*(4), 1311–1323.

Han, S., Li, Z., Ma, S., Zhi, Y., Xia, H., Chen, X., & Liu, X. (2021). Bandgap engineering in benzotrithiophene-based conjugated microporous polymers: A strategy for screening metal-free heterogeneous photocatalysts. *Journal of Materials Chemistry A*, *9*(6), 3333–3340.

Hernandezperni, G., & Leuenberger, H. (2005). The characterization of aprotic polar liquids and percolation phenomena in DMSO/water mixtures. *European Journal of Pharmaceutics and Biopharmaceutics*, *61*(3), 201–213. https://doi.org/10.1016/j.ejpb.2005.05.008

Iczkowski, R. P., & Margrave, J. L. (1961). Electronegativity. *Journal of the American Chemical Society*, *83*(17), 3547–3551. https://doi.org/10.1021/ja01478a001

Inah, B. E., Favour Azogor, N., Akpan, H. T., Levi, O. E., Charlie, D., & Adeleye, A. P. (2025). Exploring the adsorption properties of PTFE-decorated and metal doped covalent organic frameworks for environmental cleanup: A computational outlook. *Computational and Theoretical Chemistry*, *1248*, 115202. https://doi.org/10.1016/j.comptc.2025.115202

Kadhim, A., Betti, N., Al-Bahrani, H., Al-Ghezi, M., Gaaz, T., Kadhum, A., & Alamiery, A. (2021). A mini review on corrosion, inhibitors and mechanism types of mild steel inhibition in an acidic environment. *International Journal of Corrosion and Scale Inhibition*, *10*(3), 861–884.

Kasprzhitskii, A., & Lazorenko, G. (2021). Corrosion inhibition properties of small peptides: DFT and Monte Carlo simulation studies. *Journal of Molecular Liquids*, *331*, 115782.

Kaya, S., & Kaya, C. (2015). A new equation for calculation of chemical hardness of groups and molecules. *Molecular Physics*, *113*(11), 1311–1319. https://doi.org/10.1080/00268976.2014.991771

Mardirossian, N., & Head-Gordon, M. (2017). Thirty years of density functional theory in computational chemistry: An overview and extensive assessment of 200 density functionals. *Molecular Physics*, *115*(19), 2315–2372.

Marenich, A. V., Cramer, C. J., & Truhlar, D. G. (2009). Universal Solvation Model Based on Solute Electron Density and on a Continuum Model of the Solvent Defined by the Bulk Dielectric Constant and Atomic Surface Tensions. *The Journal of Physical Chemistry B*, *113*(18), 6378–6396. https://doi.org/10.1021/jp810292n

Matinise, N., Ineza, C., Oladipo, S. D., Begum, N. M., Badeji, A. A., Lopis, A. S., & Luckay, R. C. (2025). Synthesis, comprehensive characterization, crystallographic and density functional theory (DFT) studies of tridentate amic acid compounds. *Journal of Molecular Structure*, *1346*, 143220. https://doi.org/10.1016/j.molstruc.2025.143220

Minsky, A., Meyer, A. Y., & Rabinovitz, M. (1985). Paratropicity and antiaromaticity: Role of the homo-lumo energy gap. *Tetrahedron*, *41*(4), 785–791.

Murmu, M., Murmu, N. C., Ghosh, M., & Banerjee, P. (2022). Density functional theory, Monte Carlo simulation and non-covalent interaction study for exploring the adsorption and corrosion inhibiting property of double azomethine functionalised organic molecules. *Journal of Adhesion Science and Technology*, *36*(23–24), 2732–2760.

Odeyemi, O. O., & Alaba, P. A. (2025). Efficient and reliable corrosion control for subsea assets: Challenges in the design and testing of corrosion probes in aggressive marine environments. *Corrosion Reviews*, *43*(1), 79–126. https://doi.org/10.1515/corrrev-2024-0046

Oladipo, S., Adeleke, A. A., Badeji, A. A., Babalola, K. I., Labulo, A. H., Hassan, I., Yussuf, S. T., & Olalekan, S. O. (2024). Computational investigation and biological activity of selected Schiff bases. *Journal of the Nigerian Society of Physical Sciences*, 2103. https://doi.org/10.46481/jnsps.2024.2103

Oladipo, S. D., Luckay, R. C., Olofinsan, K. A., Badeji, A. A., & Mokoena, S. (2025). Exploring Schiff bases derived from 4-(diethylamino)salicylaldehyde and their copper(II) complexes as antidiabetes and antioxidant agents: Structural elucidation, DFT computational and in vitro studies. *Inorganica Chimica Acta*, *575*, 122447. https://doi.org/10.1016/j.ica.2024.122447

Omer, R. A., Azeez, Y. H., Kareem, R. O., Ahmed, L. O., & Safin, D. A. (2025). Potential Corrosion Inhibition Properties of Flavone Derivatives on the Cu(111) Surface: A Combined DFT and Monte Carlo Simulation Study. *Journal of Fluorescence*. https://doi.org/10.1007/s10895-024-04117-6

Oukhrib, R., Abdellaoui, Y., Berisha, A., Abou Oualid, H., Halili, J., Jusufi, K., Ait El Had, M., Bourzi, H., El Issami, S., Asmary, F. A., Parmar, V. S., & Len, C. (2021). DFT, Monte Carlo and molecular dynamics simulations for the prediction of corrosion inhibition efficiency of novel pyrazolylnucleosides on Cu(111) surface in acidic media. *Scientific Reports*, *11*(1), 3771. https://doi.org/10.1038/s41598-021-82927-5

Pal, R., & Chattaraj, P. K. (2023). Electrophilicity index revisited. *Journal of Computational Chemistry*, *44*(3), 278–297.

Pan, Q., Chen, X., Li, H., Chen, S., Zheng, X., Liu, H., Li, B., & Zhao, Y. (2021). Preparation of crystalline benzotrithiophene-based two-dimensional graphdiyne analogue. *2D Materials*, *9*(1), 014001.

Parr, R. G., Szentpály, L. V., & Liu, S. (1999). Electrophilicity Index. *Journal of the American Chemical Society*, *121*(9),

1922–1924. https://doi.org/10.1021/ja983494x

Patra, D., & Park, S. (2022). Solution Processable Benzotrithiophene (BTT)-Based Organic Semiconductors: Recent Advances and Review. *Macromolecular Rapid Communications*, *43*(21), 2200473.

Ramalingam, A., & Santhi, V. M. (2024). Evaluation of chemical reactivity and polarity of imidazolium-based ionic liquids using quantum chemical calculations. *Journal of Molecular Modeling*, *30*(6), 182. https://doi.org/10.1007/s00894-024-05984-3

Rossi, S., Bisello, A., Cardena, R., Orian, L., & Santi, S. (2017). Benzodithiophene and Benzotrithiophene as π Cores for Two- and Three-Blade Propeller-Shaped Ferrocenyl-Based Conjugated Systems. *European Journal of Organic Chemistry*, *2017*(40), 5966–5974. https://doi.org/10.1002/ejoc.201701045

She, X., Peng, J., Qiang, Y., Zhou, Y., & Zhang, S. (2024). Recent advances in protective technologies against copper corrosion. *Journal of Materials Science & Technology*, *201*, 75–94. https://doi.org/10.1016/j.jmst.2024.02.060

(2011) In: Materials Studio. Accelrys Software Inc., San Diego.

Su, N. Q., Zhang, I. Y., Wu, J., & Xu, X. (2011). Calculations of ionization energies and electron affinities for atoms and molecules: A comparative study with different methods. *Frontiers of Chemistry in China*, *6*(4), 269–279.

Sun, H., Ren, P., & Fried, J. R. (1998). The COMPASS force field: Parameterization and validation for phosphazenes. *Computational and Theoretical Polymer Science*, *8*(1–2), 229–246. https://doi.org/10.1016/S1089-3156(98)00042-7

Tsuneda, T., Song, J.-W., Suzuki, S., & Hirao, K. (2010). On Koopmans' theorem in density functional theory. *The Journal of Chemical Physics*, *133*(17), 174101. https://doi.org/10.1063/1.3491272

Verma, D. K., Dewangan, Y., Dewangan, A. K., & Asatkar, A. (2021). Correction to: Heteroatom-Based Compounds as Sustainable Corrosion Inhibitors: An Overview. *Journal of Bio- and Tribo-Corrosion*, *7*(2), 70. https://doi.org/10.1007/s40735-021-00509-4

Wiberg, K. B. (2004). Basis set effects on calculated geometries: 6-311++ G** vs. aug-cc-pVDZ. *Journal of Computational Chemistry*, *25*(11), 1342–1346.

Xu, X. T., Xu, H. W., Li, W., Wang, Y., & Zhang, X. Y. (2022). A combined quantum chemical, molcular dynamics and Monto Carlo study of three amino acids as corroison inhibitors for aluminum in NaCl solution. *Journal of Molecular Liquids*, *345*, 117010. https://doi.org/10.1016/j.molliq.2021.117010

Zhan, C.-G., Nichols, J. A., & Dixon, D. A. (2003). Ionization Potential, Electron Affinity, Electronegativity, Hardness, and Electron Excitation Energy: Molecular Properties from Density Functional Theory Orbital Energies. *The Journal of Physical Chemistry A*, *107*(20), 4184–4195. https://doi.org/10.1021/jp0225774

Zhang, Q., Zhang, R., Wu, R., Luo, Y., Guo, L., & He, Z. (2023). Green and high-efficiency corrosion inhibitors for metals: A review. *Journal of Adhesion Science and Technology*, *37*(9), 1501–1524.